

# Two-dimensional extended Hubbard model at half-filling

**A Sherman**

Institute of Physics, University of Tartu, W. Ostwaldi Str 1, 50411 Tartu, Estonia

E-mail: alexeisherman@gmail.com

**Abstract.** We consider the extended Hubbard model on a two-dimensional square lattice at half-filling. The model is investigated using the strong coupling diagram technique. We sum infinite series of ladder diagrams for an infinite crystal allowing for full-scale charge and spin fluctuations and the actual short-range antiferromagnetic order for nonzero temperatures. In agreement with earlier results, we find the first-order phase transition in the charge subsystem occurring at  $v = v_c \gtrsim U/4$  with  $v$  and  $U$  the intersite and on-site Coulomb repulsion constants. The state arising at the transition has alternating deviations of electron occupations from the mean value on neighboring sites. Due to fluctuations, these alternating occupation deviations have short-range order. States on transition sides differ in the sign of the zero-frequency charge susceptibility at the corner of the Brillouin zone, where it sharply peaks. For the considered parameters, such behavior is found for  $U \lesssim 5t$  with  $t$  the hopping constant. The states with alternating occupations reveal themselves in the electron density of states when it features the narrow Fermi-level peak. For the insulating case  $U \geq 7t$ , in which the transition is not observed, we find a continuous growth of the Mott gap with  $v$ .

*Keywords:* extended Hubbard model, phase transitions, strong coupling diagram technique

## 1. Introduction

The extended Hubbard model (EHM) is a generalization of the Hubbard model, which allows one to study the influence of the non-local Coulomb interaction on the properties of the strongly correlated electron system. Along with the on-site repulsion and kinetic energy, the EHM Hamiltonian contains the term describing an interaction of electrons on neighboring sites. Early studies of EHM were carried out using Monte-Carlo simulations [1, 2, 3], exact solutions for small clusters [4, 5], and mean-field approximations [6, 7]. These works demonstrated that the electron repulsion on neighboring sites leads to the phase transition in the charge subsystem occurring at  $v_c \approx U/z$ . Here  $U$  and  $v$  are Coulomb interaction constants for electrons on the same and neighboring sites, and  $z$  is the coordination number. The transition was connected with the appearance of states having alternating deviations of electron occupations from the mean value on neighboring sites (SAOs for short). Since the statistical ensemble contains states with both deviation signs, the mean site occupation remains uniform throughout the crystal. At half-filling, such deviations decrease the site spin. Therefore, the transition suppresses the antiferromagnetic ordering (AFO) of electron spins. Later on, the EHM was investigated using the extended dynamic mean-field theory (DMFT) [8], its diagrammatic extensions [9, 10], cluster generalizations of the DMFT [11], variational cluster approximation [12], and the two-particle self-consistent approach [13]. In these works, the value of  $v_c$  was refined, and the transition was shown to be of the first order.

In this work, we use the strong coupling diagram technique (SCDT) [14, 15, 16, 17] to investigate the half-filled EHM on a two-dimensional (2D) square lattice. In contrast to the above works, this approach allows us to perform calculations in an infinite crystal with the proper account of full-scale charge and spin fluctuations and the short-range AFO existing in the crystal at finite temperatures  $T$ . The adequate description of spin excitations is significant for obtaining reliable electron spectra. Another advantage of the used approach is its applicability for any non-local interaction between electrons if it is smaller than the on-site coupling.

We consider the ranges of parameters  $2t \leq U \leq 8t$ ,  $v \lesssim U/2$  and  $0.1t \lesssim T \ll U$  with  $t$  the hopping constant. To derive a closed set of SCDT equations, we sum infinite series of ladder diagrams. Self-consistent solutions of these equations are obtained by iteration. For  $U \lesssim 5t$ , we find the phase transition in the charge subsystem at  $v_c \gtrsim U/4$ . The transition reveals itself in an abrupt sign change of the zero-frequency charge susceptibility  $\chi^{\text{ch}}(\mathbf{Q}, 0)$  at the corner of the Brillouin zone  $\mathbf{Q}$ . At  $v$  near  $v_c$ , the susceptibility is sharply peaked at this momentum, which indicates that SAOs fill the bottom of the electron spectrum. The sudden sign change of  $\chi^{\text{ch}}(\mathbf{Q}, 0)$  points to a cardinal modification of the crystal electrostatic properties. It stems from the variation of the renormalized Coulomb interaction. In contrast to the mentioned mean-field approaches,  $\chi^{\text{ch}}(\mathbf{Q}, 0)$  remains finite at  $v = v_c$ , which indicates a short-range ordering of alternating occupations. The temperature dependence of the susceptibility suggests that this type of order stems from the fluctuations taken into account in this work. Another manifestation of the transition is observed for parameter sets featuring a narrow Fermi-level peak in the density of states (DOS). For  $v > v_c$ , the peak splits into two maxima due to an interaction between SAOs with opposite signs of occupation deviations, which, without this interaction, would have identical DOSs. The transition is of the first order – for  $v$  in some vicinity of  $v_c$ , two solutions with opposite signs of  $\chi^{\text{ch}}(\mathbf{Q}, 0)$  coexist. The correlation length of the short-range antiferromagnetic ordering

$\xi$  decreases monotonously with increasing  $v$ . The exception is the transition point, where a small increase of  $\xi$  is observed. Since at  $v = v_c$  site spins are decreased, this result indicates an increase in the spin exchange constant at the phase transition. For  $U \gtrsim 5t$ , it is not observed in the considered ranges of other parameters. In the case  $U \gtrsim 7t$  and  $T \approx 0.1t$ , for which DOS contains the Mott gap, the growth of  $v$  leads to a monotonous increase of its width.

The paper is organized as follows: The model Hamiltonian, a brief discussion of the SCDT, and the main formulas are given in the next section. Manifestations of the transition in determinants of the Bethe-Salpeter equations (BSE), charge susceptibility, and DOSs are treated in Sect. 3. The last section is devoted to concluding remarks.

## 2. Model and SCDT

The EHM Hamiltonian reads

$$H = \sum_{\mathbb{I}'\sigma} t_{\mathbb{I}'} a_{\mathbb{I}'\sigma}^\dagger a_{\mathbb{1}\sigma} + \frac{U}{2} \sum_{\mathbb{1}\sigma} n_{\mathbb{1}\sigma} n_{\mathbb{1},-\sigma} + \frac{1}{2} \sum_{\mathbb{I}'} v_{\mathbb{I}'} (n_{\mathbb{I}'} - \bar{n})(n_{\mathbb{1}} - \bar{n}) - \mu \sum_{\mathbb{1}} n_{\mathbb{1}}, \quad (1)$$

where  $\mathbb{1}$  and  $\mathbb{I}'$  are vectors of a 2D square lattice,  $\sigma = \pm 1$  is the spin projection,  $a_{\mathbb{1}\sigma}^\dagger$  and  $a_{\mathbb{1}\sigma}$  are electron creation and annihilation operators,  $t_{\mathbb{I}'}$ ,  $U$ , and  $v_{\mathbb{I}'}$  are constants of hopping, on-site and intersite Coulomb repulsions, respectively,  $n_{\mathbb{1}\sigma} = a_{\mathbb{1}\sigma}^\dagger a_{\mathbb{1}\sigma}$  and  $n_{\mathbb{1}} = \sum_{\sigma} n_{\mathbb{1}\sigma}$  are site occupation numbers,  $\bar{n} = \langle n_{\mathbb{1}} \rangle$  is the occupation mean value with the angle brackets denoting the statistical averaging, and  $\mu$  is the chemical potential. In this work,  $t_{\mathbb{I}'}$  and  $v_{\mathbb{I}'}$  are supposed to be nonzero for neighboring sites only,

$$t_{\mathbb{I}'} = -t \sum_{\mathbf{a}} \delta_{\mathbb{I}', \mathbb{1}+\mathbf{a}}, \quad v_{\mathbb{I}'} = v \sum_{\mathbf{a}} \delta_{\mathbb{I}', \mathbb{1}+\mathbf{a}},$$

where  $\mathbf{a}$  are four vectors connecting neighboring sites. Below, we consider the case of half-filling,  $\bar{n} = 1$ , which for the Hamiltonian (1) takes place at  $\mu = U/2$ .

For calculating Green's functions, we use the SCDT [14, 15, 16, 17]. Supposing that the on-site Coulomb repulsion is the largest energy parameter, in this approach, the local part of the Hamiltonian is considered as an unperturbed operator  $H_0$ , and correlators are calculated using series expansions in powers of nonlocal terms  $H_i$  (see, e.g., [17, 18, 19]). In the present case, the on-site Coulomb interaction and the chemical-potential term of the Hamiltonian (1) form  $H_0$ , while other parts  $H_i$ . Terms of the SCDT series are products of the hopping and intersite Coulomb interaction constants and on-site cumulants [20] of electron creation and annihilation operators. We consider terms with cumulants of the first and second orders only. This approximation was enough to obtain quantitatively correct results in the Hubbard model [17, 21]. These cumulants are constructed from a pair and two pairs of creation and annihilation operators,

$$\begin{aligned} C^{(1)}(\tau', \tau) &= \langle \mathcal{T} \bar{a}_{\mathbb{1}\sigma}(\tau') a_{\mathbb{1}\sigma}(\tau) \rangle_0, \\ C^{(2)}(\tau_1, \sigma_1; \tau_2, \sigma_2; \tau_3, \sigma_3; \tau_4, \sigma_4) &= \langle \mathcal{T} \bar{a}_{\mathbb{1}\sigma_1}(\tau_1) a_{\mathbb{1}\sigma_2}(\tau_2) \bar{a}_{\mathbb{1}\sigma_3}(\tau_3) a_{\mathbb{1}\sigma_4}(\tau_4) \rangle_0 \\ &\quad - \langle \mathcal{T} \bar{a}_{\mathbb{1}\sigma_1}(\tau_1) a_{\mathbb{1}\sigma_2}(\tau_2) \rangle_0 \langle \mathcal{T} \bar{a}_{\mathbb{1}\sigma_3}(\tau_3) a_{\mathbb{1}\sigma_4}(\tau_4) \rangle_0 \\ &\quad + \langle \mathcal{T} \bar{a}_{\mathbb{1}\sigma_1}(\tau_1) a_{\mathbb{1}\sigma_4}(\tau_4) \rangle_0 \langle \mathcal{T} \bar{a}_{\mathbb{1}\sigma_3}(\tau_3) a_{\mathbb{1}\sigma_2}(\tau_2) \rangle_0. \end{aligned}$$

The subscript 0 at angle brackets indicates that time dependencies of operators and the statistical averaging are determined by the site Hamiltonian

$$H_1 = \sum_{\sigma} [(U/2)n_{1\sigma}n_{1,-\sigma} - \mu n_{1\sigma}].$$

The sum of the site Hamiltonians forms  $H_0$ . The symbol  $\mathcal{T}$  is the chronological operator.

The terms of the SCDT series expansion can be visualized by depicting  $t_{1\nu}$  as directed lines,  $v_{1\nu}$  as crosses, and cumulants as circles. The number of lines outgoing from and incoming to the circle indicates the number of electron operators in the cumulant. As for the weak coupling diagram technique [22], the linked-cluster theorem is valid and partial summations are allowed in the SCDT. The notion of the one-particle irreducible diagram can also be introduced in this diagram technique. It is a two-leg diagram, which cannot be divided into two disconnected parts by cutting a hopping line  $t_{1\nu}$ . If we denote the sum of all such diagrams – the irreducible part – by the symbol  $K$ , the Fourier transform of the electron Green's function  $G(\mathbf{l}\tau', \mathbf{l}\tau) = \langle \mathcal{T} \bar{a}_{\mathbf{l}\sigma}(\tau') a_{\mathbf{l}\sigma}(\tau) \rangle$  can be written as

$$G(\mathbf{k}, j) = \{ [K(\mathbf{k}, j)]^{-1} - t_{\mathbf{k}} \}^{-1}. \quad (2)$$

Here  $\mathbf{k}$  is the 2D wave vector and the integer  $j$  defines the Matsubara frequency  $\omega_j = (2j - 1)\pi T$ .

Diagrams taken into account in the present calculations are shown in Fig. 1. Here short arrows entering and leaving cumulants and vertices shown by squares are their endpoints, the solid arrowed lines connecting these endpoints are the renormalized hopping

$$\theta(\mathbf{k}, j) = t_{\mathbf{k}} + t_{\mathbf{k}}^2 G(\mathbf{k}, j), \quad (3)$$

the dashed cross with an open square in the center is the bare intersite Coulomb repulsion  $v_{\mathbf{k}}$ , and the similar cross with a greyed square is the renormalized Coulomb interaction, Fig. 1(c),

$$\varphi(\mathbf{k}, \nu) = \frac{v_{\mathbf{k}}}{1 - 2v_{\mathbf{k}}TN^{-1} \sum_{\mathbf{q}j} G(\mathbf{q}, j)G(\mathbf{k} + \mathbf{q}, \nu + j)}. \quad (4)$$

Here  $N$  is the number of sites. Algebraically diagrams in Fig. 1(a) read

$$\begin{aligned} K(\mathbf{k}, j) &= C^{(1)}(j) + \frac{T^2}{4N} \sum_{\mathbf{k}'j'\nu} \theta(\mathbf{k}', j') \mathcal{T}_{\mathbf{k}-\mathbf{k}'}(j + \nu, j' + \nu) \\ &\quad \times [3C^{(a)}(j, j + \nu, j' + \nu, j') C^{(a)}(j + \nu, j, j', j' + \nu) \\ &\quad + C^{(s)}(j, j + \nu, j' + \nu, j') C^{(s)}(j + \nu, j, j', j' + \nu)] \\ &\quad - \frac{T}{2N} \sum_{\mathbf{k}'j'} \theta(\mathbf{k}', j') [3\tilde{V}_{\mathbf{k}-\mathbf{k}'}^{(a)}(j, j, j', j') \\ &\quad + \tilde{V}_{\mathbf{k}-\mathbf{k}'}^{(s)}(j, j, j', j')], \end{aligned} \quad (5)$$

where  $\mathcal{T}_{\mathbf{k}}(j, j') = N^{-1} \sum_{\mathbf{k}'} \theta(\mathbf{k} + \mathbf{k}', j) \theta(\mathbf{k}', j')$ ,  $C^{(s)}$  and  $C^{(a)}$  are second-order cumulants symmetrized and antisymmetrized over spin indices,

$$\begin{aligned} C^{(s)}(j + \nu, j, j', j' + \nu) &= \sum_{\sigma'} C^{(2)}(j + \nu, \sigma'; j, \sigma; j', \sigma; j' + \nu, \sigma') \\ C^{(a)}(j + \nu, j, j', j' + \nu) &= \sum_{\sigma'} \sigma \sigma' C^{(2)}(j + \nu, \sigma'; j, \sigma; j', \sigma; j' + \nu, \sigma'), \end{aligned} \quad (6)$$

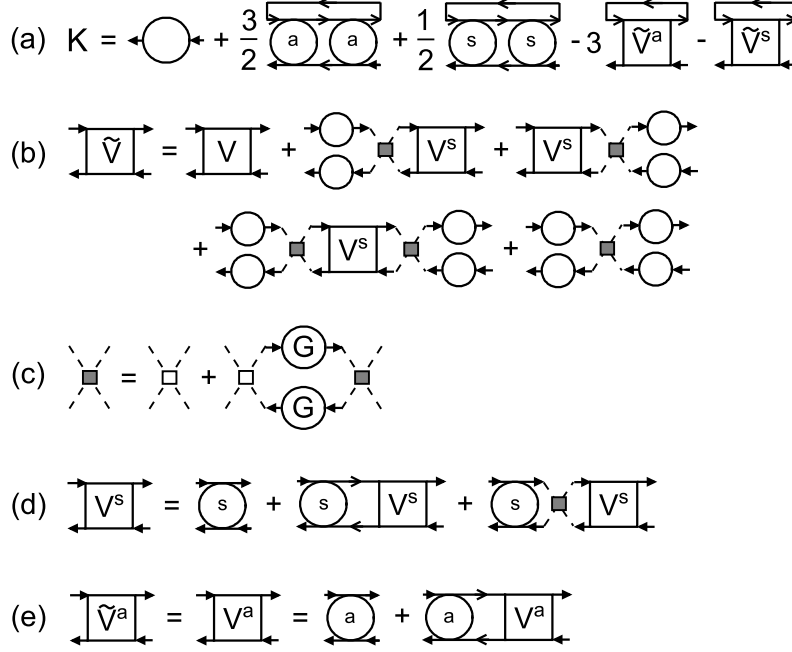


**Figure 1.** The diagrammatic representation of main equations. Open circles with one incoming and one outgoing arrows are first-order cumulants, circles with letters  $s$  and  $a$  are symmetrized and antisymmetrized second-order cumulants, circles with the letter  $G$  are Green's functions, arrowed solid lines are renormalized hopping  $\theta(\mathbf{k}, j)$ , Eq. (3), dashed crosses with open small squares are bare intersite Coulomb vertices  $v_{\mathbf{k}}$ , crosses with greyed squares are renormalized vertices  $\varphi(\mathbf{k}, j)$ , Eq. (4), squares with letters  $\tilde{V}^s$ ,  $V^s$ ,  $\tilde{V}^a$  and  $V^a$  are infinite sums of ladder diagrams in part (b) symmetrized and antisymmetrized over spin indices, Eqs. (7)–(10).

quantities  $\tilde{V}^{(s)}$  and  $\tilde{V}^{(a)}$  are results of the analogous symmetrization and antisymmetrization of the infinite sum of ladder diagrams  $\tilde{V}$  in Fig. 1(b). Two-particle irreducible vertices in this sum are the renormalized Coulomb vertices (4) and second-order cumulants. If the former vertices allow for the intersite Coulomb interaction, the latter describe the on-site coupling. All possible sequences of these vertices are taken into account,

$$\begin{aligned}
\tilde{V}_{\mathbf{k}}^{(s)}(j + \nu, j, j', j' + \nu) &= V_{\mathbf{k}}^{(s)}(j + \nu, j, j', j' + \nu) \\
&+ C^{(1)}(j + \nu)C^{(1)}(j' + \nu)\varphi(\mathbf{k}, j - j') \\
&\times T \sum_{\nu'} V_{\mathbf{k}}^{(s)}(j + \nu', j, j', j' + \nu') \\
&+ C^{(1)}(j)C^{(1)}(j')\varphi(\mathbf{k}, j - j') \\
&\times T \sum_{\nu'} V_{\mathbf{k}}^{(s)}(j + \nu, j + \nu', j' + \nu', j' + \nu) \\
&+ 2C^{(1)}(j + \nu)C^{(1)}(j' + \nu)C^{(1)}(j)C^{(1)}(j')\varphi^2(\mathbf{k}, j - j') \\
&\times T^2 \sum_{\nu'\nu''} V_{\mathbf{k}}^{(s)}(j + \nu', j + \nu'', j' + \nu'', j' + \nu')
\end{aligned}$$

$$+ C^{(1)}(j + \nu)C^{(1)}(j' + \nu)C^{(1)}(j)C^{(1)}(j')\varphi(\mathbf{k}, j - j'), \quad (7)$$

$$\tilde{V}_{\mathbf{k}}^{(a)}(j + \nu, j, j', j' + \nu) = V_{\mathbf{k}}^{(a)}(j + \nu, j, j', j' + \nu). \quad (8)$$

Here  $V^{(s)}$  and  $V^{(a)}$  are parts of these ladders, which start and finish with the second-order cumulants, Fig. 1(d) and (e),

$$\begin{aligned} V_{\mathbf{k}}^{(s)}(j + \nu, j, j', j' + \nu) &= C^{(s)}(j + \nu, j, j', j' + \nu) \\ &+ T \sum_{\nu'} C^{(s)}(j + \nu, j + \nu', j' + \nu', j' + \nu) \mathcal{T}_{\mathbf{k}}(j + \nu', j' + \nu') \\ &\quad \times V_{\mathbf{k}}^{(s)}(j + \nu', j, j', j' + \nu') \\ &+ 2T^2 \sum_{\nu' \nu''} C^{(s)}(j + \nu, j + \nu', j' + \nu', j' + \nu) \varphi(\mathbf{k}, j - j') \\ &\quad \times V_{\mathbf{k}}^{(s)}(j + \nu'', j, j', j' + \nu'') \end{aligned} \quad (9)$$

$$\begin{aligned} V_{\mathbf{k}}^{(a)}(j + \nu, j, j', j' + \nu) &= C^{(a)}(j + \nu, j, j', j' + \nu) \\ &+ T \sum_{\nu'} C^{(a)}(j + \nu, j + \nu', j' + \nu', j' + \nu) \mathcal{T}_{\mathbf{k}}(j + \nu', j' + \nu') \\ &\quad \times V_{\mathbf{k}}^{(a)}(j + \nu', j, j', j' + \nu'). \end{aligned} \quad (10)$$

Reducible vertices  $\tilde{V}^{(s)}$  and  $\tilde{V}^{(a)} = V^{(a)}$  describe charge and spin fluctuations and define respective susceptibilities  $\chi^{\text{ch}}(\mathbf{l}'\tau', \mathbf{l}\tau) = \frac{1}{2} \langle \mathcal{T}(n_{\mathbf{l}'}(\tau') - \bar{n})(n_{\mathbf{l}}(\tau) - \bar{n}) \rangle$  and  $\chi^{\text{sp}}(\mathbf{l}'\tau', \mathbf{l}\tau) = \langle \mathcal{T}\bar{a}_{\mathbf{l}'\sigma}(\tau')a_{\mathbf{l},-\sigma}(\tau')\bar{a}_{\mathbf{l},-\sigma}(\tau)a_{\mathbf{l}\sigma}(\tau) \rangle$ ,

$$\begin{aligned} \chi^{\text{ch}}(\mathbf{k}, \nu) &= -\frac{T}{N} \sum_{\mathbf{q}j} G(\mathbf{k} + \mathbf{q}, \nu + j)G(\mathbf{k}, j) \\ &\quad - T^2 \sum_{jj'} F_{\mathbf{k}}(j, \nu + j)F_{\mathbf{k}}(j', \nu + j')\tilde{V}_{\mathbf{k}}^{(s)}(\nu + j, \nu + j', j', j), \end{aligned} \quad (11)$$

$$\begin{aligned} \chi^{\text{sp}}(\mathbf{k}, \nu) &= -\frac{T}{N} \sum_{\mathbf{q}j} G(\mathbf{k} + \mathbf{q}, \nu + j)G(\mathbf{k}, j) \\ &\quad - T^2 \sum_{jj'} F_{\mathbf{k}}(j, \nu + j)F_{\mathbf{k}}(j', \nu + j')V_{\mathbf{k}}^{(a)}(\nu + j, \nu + j', j', j), \end{aligned} \quad (12)$$

where  $F_{\mathbf{k}}(j, j') = N^{-1} \sum_{\mathbf{q}} \Pi(\mathbf{q}, j)\Pi(\mathbf{k} + \mathbf{q}, j')$  and  $\Pi(\mathbf{k}, j) = 1 + t_{\mathbf{k}}G(\mathbf{k}, j)$ .

Notice that the inclusion of the intersite Coulomb interaction does not directly modify Eqs. (8) and (10) for the spin vertex  $\tilde{V}^{(a)}$ . The latter equation looks similar to the respective formula in the Hubbard model [17]. In this equation, the influence of the intersite repulsion is indirect, through the modification of electron Green's functions entering into the quantity  $\mathcal{T}_{\mathbf{k}}(j, j')$ . Comparing with the Hubbard model, we see that main changes occurred in Eqs. (7) and (9) for the charge vertex  $\tilde{V}^{(s)}$ .

For calculations, the above formulas have to be supplemented by expressions for cumulants. They can be found in [14, 15, 16, 17]. These expressions can be significantly simplified in the case

$$T \ll \mu, \quad T \ll U - \mu. \quad (13)$$

For  $U \gg T$ , this range of chemical potentials contains relevant cases of half-filling,  $\mu = U/2$ , and moderate doping. In this range, cumulants read

$$C^{(1)}(j) = \frac{1}{2} [g_1(j) + g_2(j)],$$

$$\begin{aligned}
C^{(2)}(j + \nu, \sigma; j, \sigma'; j', \sigma'; j' + \nu, \sigma) &= \frac{1}{4T} [\delta_{jj'} (1 - 2\delta_{\sigma\sigma'}) \\
&+ \delta_{\nu 0} (2 - \delta_{\sigma\sigma'})] a_1(j' + \nu) a_1(j) - \frac{1}{2} \delta_{\sigma, -\sigma'} [a_1(j' + \nu) a_2(j, j') \\
&+ a_2(j' + \nu, j + \nu) a_1(j) + a_3(j' + \nu, j + \nu) a_4(j, j') \\
&+ a_4(j' + \nu, j + \nu) a_3(j, j')],
\end{aligned} \tag{14}$$

where

$$\begin{aligned}
g_1(j) &= (i\omega_j + \mu)^{-1}, \quad g_2(j) = (i\omega_j + \mu - U)^{-1}, \\
a_1(j) &= g_1(j) - g_2(j), \quad a_2(j, j') = g_1(j) g_1(j'), \\
a_3(j, j') &= g_2(j) - g_1(j'), \quad a_4(j, j') = a_1(j) g_2(j').
\end{aligned}$$

With these expressions, vertices  $V^{(s)}$  and  $V^{(a)}$  acquire the form

$$\begin{aligned}
V_{\mathbf{k}}^{(s)}(j + \nu, j, j', j' + \nu) &= \frac{1}{2} f_{\mathbf{k}}^{(2)}(j + \nu, j' + \nu) \\
&\times \{ 2C^{(s)}(j + \nu, j, j', j' + \nu) + 4a_{\mathbf{k}}(j' + \nu, j + \nu) \\
&\times [C'(j, j') + z'(\mathbf{k}, j, j')] - a_2(j' + \nu, j + \nu) z_1(\mathbf{k}, j, j') \\
&- a_1(j' + \nu) z_2(\mathbf{k}, j, j') - a_4(j' + \nu, j + \nu) z_3(\mathbf{k}, j, j') \\
&- a_3(j' + \nu, j + \nu) z_4(\mathbf{k}, j, j') \}
\end{aligned} \tag{15}$$

$$\begin{aligned}
V_{\mathbf{k}}^{(a)}(j + \nu, j, j', j' + \nu) &= \frac{1}{2} f_{\mathbf{k}}^{(1)}(j + \nu, j' + \nu) \\
&\times \{ 2C^{(a)}(j + \nu, j, j', j' + \nu) + [a_2(j' + \nu, j + \nu) \\
&- T^{-1} \delta_{jj'} a_1(j' + \nu)] y_1(\mathbf{k}, j, j') + a_1(j' + \nu) y_2(\mathbf{k}, j, j') \\
&+ a_4(j' + \nu, j + \nu) y_3(\mathbf{k}, j, j') + a_3(j' + \nu, j + \nu) y_4(\mathbf{k}, j, j') \}.
\end{aligned} \tag{16}$$

The BSE (9) and (10) are transformed into two small systems of linear equations. Each system has four equations with four unknowns  $z_i(\mathbf{k}, j, j')$  or  $y_i(\mathbf{k}, j, j')$ ,  $i = 1, \dots, 4$ , for fixed  $\mathbf{k}$ ,  $j$  and  $j'$ ,

$$\begin{aligned}
z_i(\mathbf{k}, j, j') &= d_i(\mathbf{k}, j, j') - e_{i2}(\mathbf{k}, j - j') z_1(\mathbf{k}, j, j') \\
&- [e_{i1}(\mathbf{k}, j - j') - p_i(\mathbf{k}, j - j')] z_2(\mathbf{k}, j, j') \\
&- [e_{i4}(\mathbf{k}, j - j') - (i\omega_j - i\omega_{j'} - U)^{-1} p_i(\mathbf{k}, j - j')] z_3(\mathbf{k}, j, j') \\
&- [e_{i3}(\mathbf{k}, j - j') + p_i(\mathbf{k}, j - j')] z_4(\mathbf{k}, j, j'),
\end{aligned} \tag{17}$$

$$\begin{aligned}
y_i(\mathbf{k}, j, j') &= b_i(\mathbf{k}, j, j') + [c_{i2}(\mathbf{k}, j - j') - T^{-1} \delta_{jj'} c_{i1}(\mathbf{k}, j - j')] \\
&\times y_1(\mathbf{k}, j, j') + c_{i1}(\mathbf{k}, j - j') y_2(\mathbf{k}, j, j') + e_{i4}(\mathbf{k}, j - j') y_3(\mathbf{k}, j, j') \\
&+ c_{i3}(\mathbf{k}, j - j') y_4(\mathbf{k}, j, j').
\end{aligned} \tag{18}$$

Hence the BSE equations (9) and (10) can be exactly solved. In the above relations

$$\begin{aligned}
f_{\mathbf{k}}^{(1)}(j, j') &= \left[ 1 + \frac{1}{4} a_1(j) a_1(j') \mathcal{T}_{\mathbf{k}}(j, j') \right], \\
f_{\mathbf{k}}^{(2)}(j, j') &= \left[ 1 - \frac{3}{4} a_1(j) a_1(j') \mathcal{T}_{\mathbf{k}}(j, j') \right], \\
C'(j, j') &= T \sum_{\nu} C^{(s)}(j + \nu, j, j', j' + \nu) \\
&= \frac{1}{4} \left[ a_2(j, j') - a_4(j, j') + \frac{a_3(j, j')}{i\omega_j - i\omega_{j'} - U} \right],
\end{aligned}$$

$$\begin{aligned}
C''(j-j') &= T \sum_{\nu} C'(j+\nu, j'+\nu) = \frac{U/2}{(\omega_j - \omega_{j'})^2 + U^2}, \\
a_{\mathbf{k}}(j, j') &= \frac{\varphi(\mathbf{k}, j-j')C'(j, j')}{1 - 2C''(j-j')\varphi(\mathbf{k}, j-j')}, \\
z'(\mathbf{k}, j, j') &= \frac{1}{4} \left[ z_2(\mathbf{k}, j, j') - z_4(\mathbf{k}, j, j') + \frac{z_3(\mathbf{k}, j, j')}{i\omega_j - i\omega_{j'} - U} \right], \\
e_{ii'}(\mathbf{k}, \nu) &= \frac{T}{2} \sum_j a_i(\nu+j, j) a_{i'}(j, \nu+j) \mathcal{T}_{\mathbf{k}}(\nu+j, j) f_{\mathbf{k}}^{(2)}(\nu+j, j), \\
c_{ii'}(\mathbf{k}, \nu) &= \frac{T}{2} \sum_j a_i(\nu+j, j) a_{i'}(j, \nu+j) \mathcal{T}_{\mathbf{k}}(\nu+j, j) f_{\mathbf{k}}^{(1)}(\nu+j, j), \\
p_i(\mathbf{k}, \nu) &= \frac{\varphi(\mathbf{k}, \nu)}{4[1 - 2C''(\nu)\varphi(\mathbf{k}, \nu)]} \\
&\quad \times \left[ e_{i2}(\mathbf{k}, \nu) - e_{i4}(\mathbf{k}, \nu) - \frac{e_{i3}(\mathbf{k}, \nu)}{i\omega_{j'} - i\omega_j - U} \right], \\
d_i(\mathbf{k}, j, j') &= \frac{3}{4} a_i(j, j') a_1(j) a_1(j') \mathcal{T}_{\mathbf{k}}(j, j') f_{\mathbf{k}}^{(2)}(j, j') \\
&\quad - e_{i1}(\mathbf{k}, j-j') a_2(j, j') - e_{i2}(\mathbf{k}, j-j') a_1(j) \\
&\quad - e_{i3}(\mathbf{k}, j-j') a_4(j, j') - e_{i4}(\mathbf{k}, j-j') a_3(j, j') \\
&\quad + 4p_i(\mathbf{k}, j-j') C'(j, j'), \\
b_i(\mathbf{k}, j, j') &= -\frac{1}{4} a_i(j, j') a_1(j) a_1(j') \mathcal{T}_{\mathbf{k}}(j, j') f_{\mathbf{k}}^{(1)}(j, j') \\
&\quad + c_{i1}(\mathbf{k}, j-j') [a_2(j, j') - T^{-1} \delta_{jj'} a_1(j)] + c_{i2}(\mathbf{k}, j-j') a_1(j) \\
&\quad + c_{i3}(\mathbf{k}, j-j') a_4(j, j') + c_{i4}(\mathbf{k}, j-j') a_3(j, j').
\end{aligned}$$

The above equations form a closed set allowing one to find the electron Green's function by iteration for given values of  $U/t$ ,  $T/t$ ,  $\mu/t$ , and functions  $t_{\mathbf{k}}$ ,  $v_{\mathbf{k}}$ . The iteration procedure appears as follows: the initial or obtained in the previous step irreducible part  $K(\mathbf{k}, j)$  is used for calculating the Green's function (2). The latter is applied for finding the renormalized hopping (3), renormalized interaction (4), and coefficients in the BSE equations (17) and (18). After their solution, we can calculate vertices (15) and (16), from which the new function  $K(\mathbf{k}, j)$  is derived from Eq. (5). The procedure is continued until convergence. As the starting function  $K$  in this iteration, we used  $C^{(1)}(j)$ , the first term in this equation. It is the irreducible part of the Hubbard-I approximation [14]. Investigating the order of the transition in the charge subsystem, we shall also use other iteration procedures, which will be discussed in the next section.

It should be underlined that the above equations are derived for an infinite crystal, and the results obtained with them belong to this crystal. To perform summations over wave vectors, we use an  $8 \times 8$  mesh. Its application is a method of approximate integration.

The calculations were carried out for  $2t \leq U \leq 8t$ ,  $v \lesssim U/2$  and temperatures  $0.1t \lesssim T \ll U$  to satisfy the condition (13) for  $\mu = U/2$ .

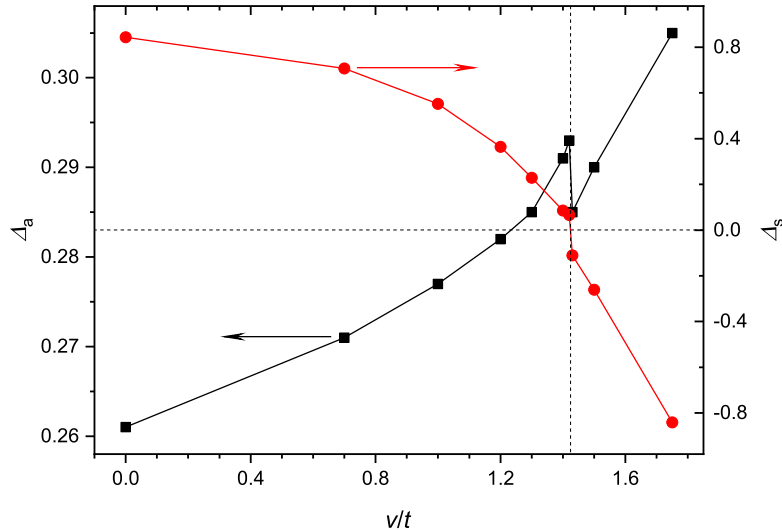


**Figure 2.** Dependencies of the determinants  $\Delta_s(\mathbf{k}, \nu)$  and  $\Delta_a(\mathbf{k}, \nu)$  of the systems of linear equations (17) and (18) on the intersite interaction constant  $v$  for  $\mathbf{k} = \mathbf{Q}$ ,  $\nu = 0$ ,  $U = 4t$ ,  $T = 0.096t$ . Red circles show calculated results for  $\Delta_s$ , the right coordinate axis. Black squares are data for  $\Delta_a$ , the left axis. The solid lines are a guide to the eye. The vertical dashed line indicates the location of the transition.

### 3. Results

#### 3.1. Determinants

Phase transitions occur when the two-particle correlators  $\tilde{V}^{(s)}$  and  $\tilde{V}^{(a)}$  diverge or change discontinuously [22]. As follows from Eqs. (7) and (8), the sources of such changes may be the renormalized Coulomb interaction  $\varphi$  or vertices  $V^{(s)}$  and  $V^{(a)}$ . Simple calculations show that the denominator in Eq. (4) can vanish in the parameter range of interest. Indeed, let us approximate Green's function in this equation by the first-order cumulant (14). This approximation corresponds to the case  $t \ll U$ . Performing the summation over Matsubara frequencies in (4), we find that the denominator vanishes at  $v = U/4$ ,  $\nu = 0$ , and  $\mathbf{k} = \mathbf{Q} = (\pi/a, \pi/a)$  with  $a = |\mathbf{a}|$ . It is the result of the mean-field approximation [6, 7]. However, Green's functions obtained in our calculations differ significantly from  $C^{(1)}$ . We did not observe the divergence of  $\varphi$  for any of the considered sets of parameters. All found divergencies and discontinuities were connected with the vertices  $V^{(s)}$  and  $V^{(a)}$ .

The BSEs (9) and (10) are linear systems of equations, and discontinuities in their solutions are defined by their determinants  $\Delta_s(\mathbf{k}, \nu)$  and  $\Delta_a(\mathbf{k}, \nu)$ , for the stationary case at  $\nu = 0$ . The value of  $\mathbf{k}$ , for which a discontinuity occurs, defines the character of the ordered state. In the Hubbard model,  $\Delta_a(\mathbf{k}, \nu)$  vanishes for  $T \rightarrow 0$  at  $\mathbf{k} = \mathbf{Q}$ ,  $\nu = 0$  and half-filling [17]. This behavior signals the transition from the short-range to the long-range AFO. In this model, in the range of chemical potentials (13),  $\Delta_s(\mathbf{k}, 0)$  varies slowly near unity.

Above, we reduced the complex BSEs (9) and (10) to two systems (17) and (18) containing every four equations. One can easily calculate their determinants. Results of such calculations for one of the parameter sets are shown in Fig. 2. The

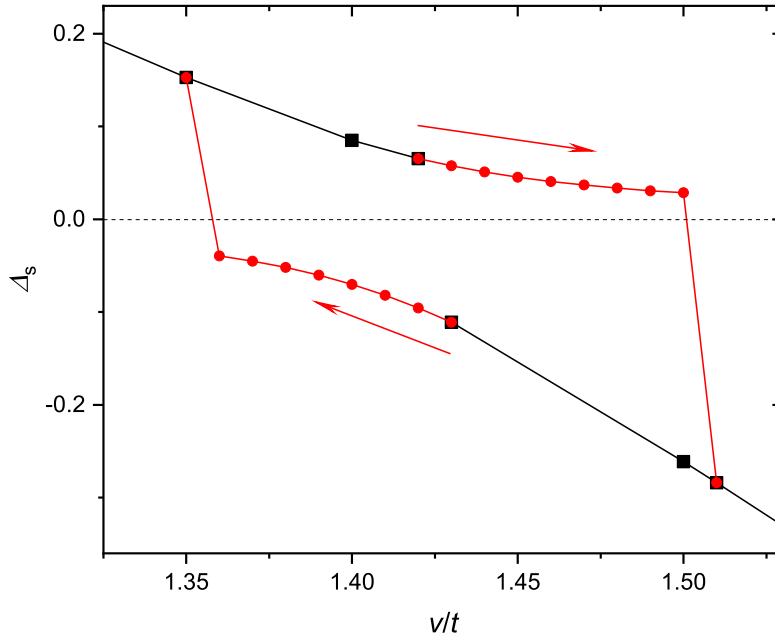


**Figure 3.** The dependence of the determinant  $\Delta_s(\mathbf{Q}, 0)$  on  $v$ . Results obtained with the initial  $K(\mathbf{k}, j) = C^{(1)}(j)$  are shown by black squares. Red circles correspond to solutions derived by a gradual variation of  $v$  from the former results with  $v$  closest to  $v_c$ . Change directions are shown by arrows.  $U = 4t$ ,  $T = 0.096t$ . The lines are a guide to the eye.

determinants for  $\mathbf{k} = \mathbf{Q}$  and  $\nu = 0$  are depicted since abrupt changes in  $\Delta_s$  occur at these momentum and frequency. On the other hand,  $\Delta_a(\mathbf{Q}, 0)$  is the probe for the antiferromagnetic ordering since  $\chi^{\text{sp}}(\mathbf{Q}, 0) \sim 1/\Delta_a(\mathbf{Q}, 0)$ . As seen from the figure,  $\Delta_s(\mathbf{Q}, 0)$  abruptly changes sign at  $v = v_c \approx 1.425t$ . We observed similar discontinuities of this determinant for other parameters in the range of the on-site repulsions  $2t \leq U \lesssim 5t$ . Smaller values of  $U$  were not considered. For larger on-site repulsions, we did not find such behavior of the denominator for  $v \lesssim U/2$  and  $T \ll U$ .

This abrupt change in  $\Delta_s(\mathbf{Q}, 0)$  points to a phase transition in the charge subsystem. As will be seen below, the transition manifests itself in the susceptibility  $\chi^{\text{ch}}(\mathbf{k}, 0)$ , which is sharply peaked at  $\mathbf{k} = \mathbf{Q}$  for  $v \approx v_c$  and changes sign at the transition. From earlier results, we know that this behavior is connected with the appearance of SAOs at the bottom of the electron spectrum.

We noticed that the sign change in  $\Delta_s$  occurs abruptly. Indeed, if we try to come close to a transition point, we obtain a solution with either positive or negative  $\Delta_s(\mathbf{Q}, 0)$  and never with a negligibly small value. This result points to the first-order transition. To prove this supposition, we obtained solutions in the transition region in a somewhat different manner. As indicated above, we mainly use iteration starting from  $K(\mathbf{k}, j) = C^{(1)}(j)$ . Now we use such obtained solutions, which are the closest to a transition point, as starting ones in iteration, in which we gradually vary  $v$ . This parameter is changed in the direction of the opposite side of the transition. That is, if, for example, we take a solution with  $v > v_c$  as initial, this constant is slightly decreased. After achieving the convergence, the obtained  $K$  is used as the starting one in the next

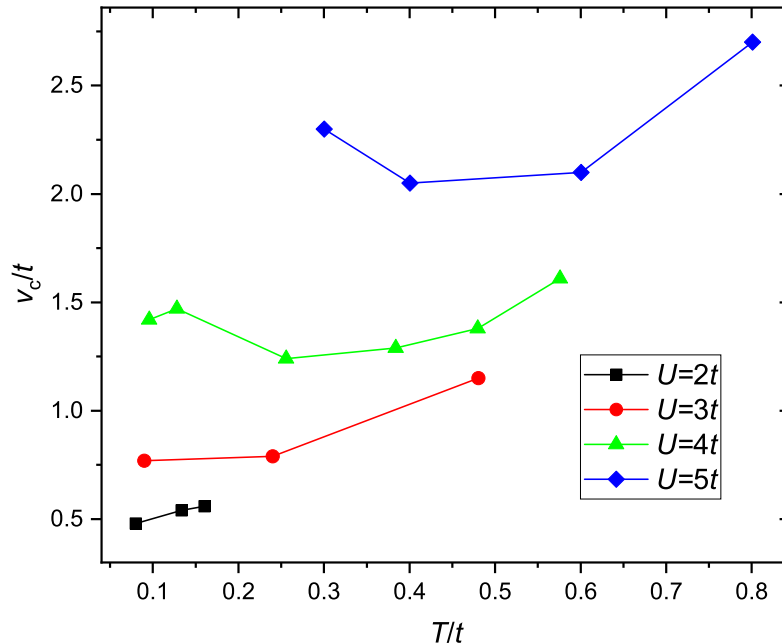


**Figure 4.** The dependence of the critical value  $v_c$  on the temperature  $T$  and on-site repulsion  $U$ . Symbols show calculated results, lines are a guide to the eye.

iteration with an even smaller  $v$ . The determinants  $\Delta_s(\mathbf{Q}, 0)$  of such obtained solutions are shown in Fig. 3. As follows from the figure, in the range  $1.36t \leq v \leq 1.5t$  there are two coexisting solutions with opposite signs of the determinant. This coexistence is inherent in the first-order transitions. Similar behavior is also observed for other considered parameter sets with  $U \lesssim 5t$ . The conclusion about the transition order agrees with results of previous works [8, 9, 10, 11, 12, 13].

As seen from Fig. 3, with this new iteration scheme, values of  $\Delta_s$  have noticeably reduced. Nevertheless, they remained nonzero, and their leveling at non-vanishing values is seen in the figure. Hence, the vertex  $V^{(s)}(\mathbf{Q}, 0)$  and the susceptibility  $\chi^{\text{ch}}(\mathbf{Q}, 0)$  do not diverge at the transition. It means that the state established in the transition has short-range ordering. Similar behavior was observed for other considered sets of parameters. However, for higher temperatures, values of  $|\Delta_s(\mathbf{Q}, 0)|$  at  $v = v_c$  appeared to be much smaller than for lower  $T$ . For example, for  $U = 4t$  and  $T = 0.58t$ , this parameter is approximately four times smaller than at  $T = 0.096t$ . Since the charge and spin fluctuations fall off with growing  $T$ , this result indicates that they are responsible for the short-range ordering of the state at  $v > v_c$ .

Figure 4 demonstrates the dependence of the critical value  $v_c$  on the temperature  $T$  and on-site repulsion  $U$ . These values were obtained in iteration with the starting irreducible part  $K(\mathbf{k}, j) = C^{(1)}(j)$ . For  $U = 2t, 3t$  and  $4t$  temperatures lower than shown in the figure were not considered. For  $U = 3t, 4t$  and  $5t$  temperatures higher than shown in the figure were not used since they violate the condition (13). We found no phase transitions in the cases  $U = 2t, T \gtrsim 0.16t$  and  $U = 5t, T \lesssim 0.3t$  as well as for  $U \gtrsim 5t$  in the mentioned above ranges of  $v$  and  $T$ . As seen from the figure,  $v_c$  depends rather strongly on  $T$ . For  $U = 2t$  and  $3t$ , the value  $v_c$  is close to its mean-field estimate

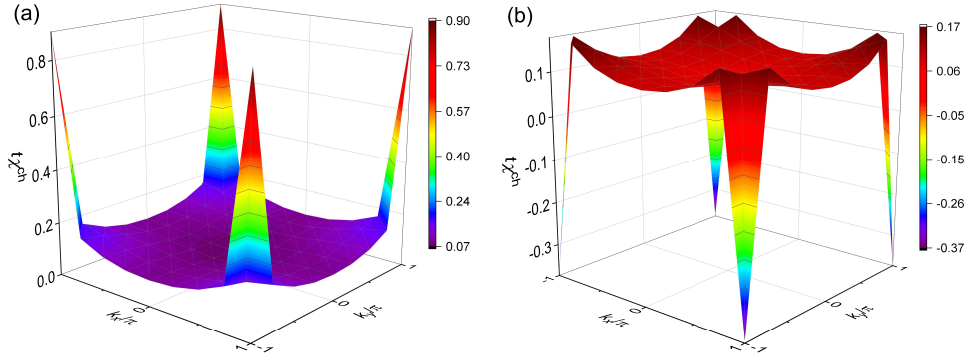


**Figure 5.** The zero-frequency charge susceptibility  $\chi^{\text{ch}}(\mathbf{k}, 0)$ , Eq. (11), as a function of the wave vector.  $U = 4t$ ,  $T = 0.096t$ ,  $v = 1.42t$  (a) and  $1.43t$  (b).

$U/4$  and somewhat exceeds it for larger  $U$ . It is close to the values obtained by other methods. However, the range  $U \lesssim 5t$ , in which we observe transition, is much smaller than the interval  $U \lesssim 9t$  obtained for  $v < U/2$  in the extended DMFT [9, 10]. To elucidate the source of this difference, let us clarify the origin of the upper bound of  $U$ . The on-site and intersite repulsions compete with each other – the former tends to the single site occupation, whereas the latter to alternating deviations from such population on neighboring sites. Therefore, for  $U > v$ , the opening of the Mott gap at  $U = U_c$  suppresses the phase transition in the charge subsystem. The value of  $U_c$  defines the range of on-site repulsions in which this transition can be observed. For  $T \approx 0.1t$ , the SCDT gives  $U_c \approx 6t$  [17]. The one-site DMFT gives the significantly overestimated [23] value  $U_c \approx 9t$ , which explains the mentioned difference.

Let us return to Fig. 2 and consider the dependence of  $\Delta_a(\mathbf{Q}, 0)$  on  $v$ . As mentioned above, this determinant is a probe of the AFO of electron spins in the system – its zero value signals the establishment of the long-range order, while quantities  $0 < \Delta_a(\mathbf{Q}, 0) \approx 1$  point to a short-range ordering. The comparatively small  $\Delta_a$  at  $v = 0$  corresponds to the antiferromagnetic correlation length  $\xi \approx 5a$ . As  $v_c$  is approached from below, the denominator grows, which points to a gradual decrease of  $\xi$ . The increase of  $v$  in this region leads to the transfer of SAOs to the lower part of the electron spectrum. In these states, occupation deviations from unity reduce site spins, which explains the decrease in  $\xi$ . The attenuation is not as strong as in small clusters [3, 11]. The difference stems from the fact that in the latter case SAOs destroy the saturated AFO of small lattices, whereas the considered infinite crystal is far from the long-range ordering. The increase of  $\Delta_a$  continues for  $v > v_c$ . However, at  $v = v_c$ , the denominator shows a small decrease. As the site spins cannot suddenly grow here, we suppose that the transition leads to an increase in the spin exchange constant  $J$ .

### 3.2. Charge susceptibility

The momentum dependence of the zero-frequency charge susceptibility  $\chi^{\text{ch}}(\mathbf{k}, 0)$ , Eq. (11), calculated for  $U = 4t$ ,  $T = 0.096t$  and  $v$  slightly smaller and larger than  $v_c \approx 1.425t$  is shown in Fig. 5. As seen from the figure, at  $\mathbf{k} = \mathbf{Q}$ , the susceptibility sharply changes sign at the transition. This modification of  $\chi^{\text{ch}}(\mathbf{k}, 0)$  is connected with

the above-discussed sign change of the determinant  $\Delta_s(\mathbf{Q}, 0)$  in the BSE (17). It is one of the manifestations of the phase transition in the charge subsystem. Analogous variations in the susceptibility are observed for other considered sets of parameters with  $U \lesssim 5t$ .

As follows from Fig. 5, for  $v \approx v_c$ , both below and above the transition, the susceptibility

$$\chi^{\text{ch}}(\mathbf{Q}, 0) = \frac{1}{2} \sum_{\mathbf{l}} \int_0^{1/T} e^{i\mathbf{Q}\mathbf{l}} \langle (n_{\mathbf{l}}(\tau) - \bar{n})(n_{\mathbf{0}} - \bar{n}) \rangle d\tau \quad (19)$$

is sharply peaked at  $\mathbf{k} = \mathbf{Q}$ . Therefore,

$$\int_0^{1/T} \langle (n_{\mathbf{l}}(\tau) - \bar{n})(n_{\mathbf{0}} - \bar{n}) \rangle d\tau \sim e^{i\mathbf{Q}\mathbf{l}} \quad (20)$$

on each side of the transition. Thus, in this region of  $v$ , occupation deviations from  $\bar{n} = 1$  have different signs on neighboring sites. It means that SAOs define the behavior of the above correlators. The susceptibility  $\chi^{\text{ch}}(\mathbf{Q}, 0)$  grows continuously when  $v$  varies from 0 to  $v_c$  where it reaches a maximum. It indicates that SAOs comprise the bottom of the electron spectrum.

Further increase of the intersite repulsion leads to the sign change in the susceptibility. This modification stems from the variation of the denominator

$$1 - 2C''(0)\varphi(\mathbf{Q}, 0) = 1 - U^{-1}\varphi(\mathbf{Q}, 0)$$

in the terms  $p_i(\mathbf{Q}, 0)$  entering into the coefficients of the BSE (17). In its turn, the value of the denominator depends on  $\varphi(\mathbf{Q}, 0)$  describing the modification of the Coulomb interaction in the crystal. Its sharp change as  $v$  crosses  $v_c$  leads to the establishment of completely different electrostatic properties. As will be seen below, this variation has also manifestations in electron DOSs.

As mentioned above, the susceptibility does not diverge at the transition point. Finite values of  $\chi^{\text{ch}}(\mathbf{Q}, 0)$  were related to charge and spin fluctuations taken into account in this work. As a consequence, the correlator (20) decays with growing  $|\mathbf{l}|$  on either side of the transition, and the decay coefficient is determined by widths of extrema at  $\mathbf{k} = \mathbf{Q}$  in the susceptibility. Hence these states are characterized by the short-range ordering of alternating deviations of electron occupations.

The considered transition is of the first order, with a range of  $v$ , in which two solutions with different susceptibilities and DOSs coexist. The susceptibilities (19) of these coexisting solutions look similar to those shown in Fig. 5. For example, all solutions corresponding to the upper branch of the curve in Fig. 3 have susceptibilities resembling that in Fig. 5(a), while for those on the lower branch  $\chi^{\text{ch}}(\mathbf{Q}, 0)$  is akin to Fig. 5(b).

### 3.3. Density of states

In this subsection, we consider the DOS of the obtained solutions,

$$\rho(\omega) = -\frac{1}{\pi N} \sum_{\mathbf{k}} \text{Im}G(\mathbf{k}, \omega).$$

The analytic continuation to real frequencies  $\omega$  was performed using the maximum entropy method [24, 25, 26].

The evolution of the DOS with the variation of  $v$  near the critical value  $v_c$  is shown in Fig. 6. For the parameters of this figure  $v_c \approx 1.425t$ . For  $v = 0$ , the considered case

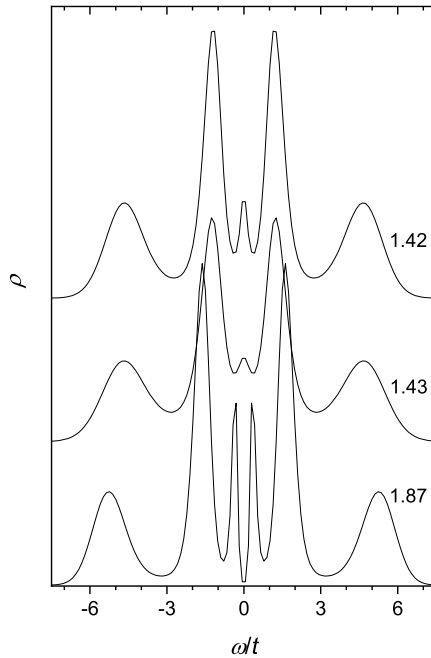


**Figure 6.** The evolution of the density of states with the variation of  $v$ .  $U = 4t$ ,  $T = 0.096t$ , values of  $v/t$  are shown near the curves.

is characterized by the Fermi-level peak [27] – the narrow spectral maximum kept near the Fermi level  $\omega = 0$  in a wide range of  $\bar{n}$  and related to a narrow band. The bound state of electrons and spin excitations form this band. By its nature, it is similar to the spin-polaron band of the  $t$ - $J$  model [28, 29, 30]. For  $v < v_c$ , the peak is still seen in the DOS (see the uppermost curve in Fig. 6). However, for larger  $v$ , the peak splits into two maxima (see the DOS for  $v = 1.87t$ ). Since spin correlations fall off with growing  $v$ , this splitting cannot be explained by the Slater mechanism [31]. We relate the splitting to SAOs becoming the ground states for these intersite repulsions. The system has two types of such states – one group with an increased population on even sites and decreased on odd ones and another group with the opposite distribution of electrons. If these two groups of states did not interact with each other, they would have the same DOSs with Fermi-level peaks. Since such interaction exists, narrow peaks split, and broad bands widen, as seen in Fig. 6. Similar behavior is observed for  $U = 2t$ ,  $T = 0.08t$ . For higher temperatures and moderate on-site repulsions, spectral maxima are broad. In these cases, only their widening occur with increasing  $v$ .

As mentioned above, in the considered ranges of parameters, we found no phase transitions and manifestations of SAOs for  $U \gtrsim 5t$ . Respectively, the influence of the intersite repulsion on spectra is weaker in this case. An example of such changes is shown in Fig. 7 for  $U = 8t$ ,  $T = 0.13t$ . The main spectral modification caused by increasing  $v$  is a tiny growth of the Mott gap with small variations in DOS shapes. One can expect the gain in the gap width as  $v$  grows from the fact that for  $v \gg U, t$ , the system is an insulator with the gap  $\sim 8v$ . Indeed, in this case, the lowest states are formed from nearly empty and doubly occupied site states. The transfer of an electron from a doubly occupied to an empty site needs the energy input of  $8v$ . Figure 7 shows

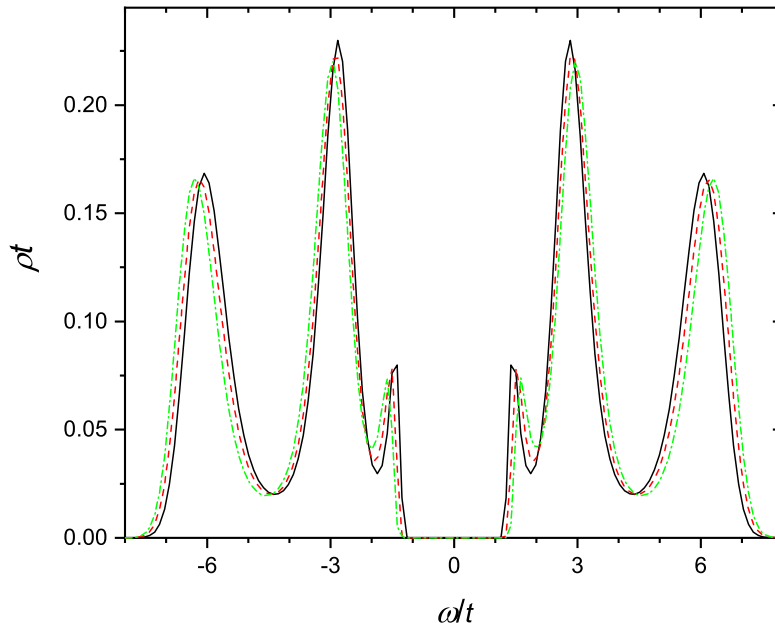


**Figure 7.** Same as in Fig. 6, but for  $U = 8t$ ,  $T = 0.13t$ . The black solid, red dashed, and green dash-dotted lines correspond to  $v = 0$ ,  $1.78t$ , and  $3t$ , respectively.

that the gap increases already starting from small  $v$ . This result contradicts the data obtained with the extended DMFT. In the latter approach, the gap decreases for  $v \lesssim U$  [9]. In the cluster DMFT [11], the gap grows with  $v$  as in our results in Fig. 7. However, in this approach, the used small cluster is in the saturated antiferromagnetic state for moderate temperatures. Consequently, even for moderate  $U$ , the Slater gap [31] is observed for small  $v$  instead of the Fermi-level peak. The gap width grows with  $v$  and transforms gradually to the intersite-repulsion gap.

#### 4. Conclusion

In this work, we used the strong coupling diagram technique for investigating the extended Hubbard model at half-filling. This approach applies the series expansion over the kinetic and intersite repulsion terms for calculating Green's functions. We summed infinite series of diagrams for an infinite two-dimensional square lattice. It allowed us to take proper account of spin and charge fluctuations and actual short-range antiferromagnetic ordering existing in the crystal for finite temperatures. The ranges of the on-site Coulomb repulsion  $2t \leq U \leq 8t$ , intersite interaction  $0 \leq v \lesssim U/2$  and temperature  $0.1t \lesssim T \ll U$  were considered. Here  $t$  is the hopping constant between neighboring sites. We found that for  $U \lesssim 5t$  the zero-frequency charge susceptibility at the corner of the Brillouin zone  $\chi^{\text{ch}}(\mathbf{Q}, 0)$  abruptly changes sign at  $v = v_c \gtrsim U/4$ . The susceptibility does not diverge at this value of the intersite repulsion; however, it peaks sharply at the momentum  $\mathbf{k} = \mathbf{Q}$ . It indicates that states with alternating deviations from the mean occupation on neighboring sites comprise the bottom of the electron spectrum for  $v$  near  $v_c$ . The change in the

susceptibility points to the cardinal modification in the crystal electrostatic properties at the transition. It is connected with the variation in the renormalized Coulomb interaction occurring at  $v = v_c$ . The transition is of the first order – in some vicinity of the transition point, solutions with both susceptibility signs coexist. As follows from the temperature dependence of determinants of the Bethe-Salpeter equation, finite values of the charge susceptibility at  $v = v_c$  are a consequence of charge and spin fluctuations taken into account in our approach. Hence the transition occurs into the state with the short-range ordering of alternating populations, and its correlation length is defined by the width of the minimum in  $\chi^{\text{ch}}(\mathbf{k}, 0)$  at  $\mathbf{k} = \mathbf{Q}$ . This result differs from works using mean-field approximations, in which the susceptibility diverges, and the state at  $v > v_c$  has the long-range order. The growth of  $v$  leads to the decay of antiferromagnetic spin correlations. The exclusion is the transition point, where a slight increase of the zero-frequency spin susceptibility at  $\mathbf{k} = \mathbf{Q}$  is observed. Since the crystal state is sharply changed at this point, we relate this increase to a growth of the exchange constant. Manifestations of states with alternating populations at  $v \geq v_c$  can also be observed in the density of electron states  $\rho(\omega)$ . In the Hubbard model, for moderate  $U$  and  $T$ ,  $\rho$  contains a sharp Fermi-level peak at  $\omega = 0$ . This peak is seen up to  $v = v_c$ . For larger  $v$ , it splits into two maxima. Qualitatively this splitting can be understood as follows: For  $v > v_c$ , there exist two sets of low-lying states with alternating populations, in one of which increased occupations are located on even sites and in the other on odd ones. Without an interaction between these two sets, identical densities of states would correspond to them. Calculated results show that this interaction exists and splits narrow peaks. In the insulating cases  $U \geq 7t$  and  $T \approx 0.1t$ , for which we found no transitions in the charge subsystem in the considered range of parameters, a monotonous growth of the Mott gap with increasing  $v$  is observed.

## References

- [1] Hirsch J E 1984 *Phys. Rev. Lett.* **53** 2327
- [2] Lin H Q and Hirsch J E *Phys. Rev. B* **33** 8155
- [3] Zhang Y and Callaway J 1989 *Phys. Rev. B* **39** 9397
- [4] Fourcade B and Spronken G 1984 *Phys. Rev. B* **29** 5096
- [5] del Bosch L M and Falicov L M 1988 *Phys. Rev. B* **37** 6073
- [6] Yan Xin-Zhong 1993 *Phys. Rev. B* **48** 7140
- [7] Dagotto E, Riera J, Chen Y C, Moreo A, Nazarenko A, Alcaraz F and Ortolani F 1994 *Phys. Rev. B* **49** 3548
- [8] Sun Ping and G Kotliar 2002 *Phys. Rev. B* **66** 085120
- [9] Ayrat T, Biermann S and Werner P 2013 *Phys. Rev. B* **87** 125149
- [10] Loon E G C P, Lichtenstein A I, Katsnelson M I, Parcollet O and Hafermann H 2014 *Phys. Rev. B* **90** 235135
- [11] Paki J, Terletska H, Isakov S and Gull E 2019 *Phys. Rev. B* **99** 245146
- [12] Aichhorn M, Evertz H G, von der Linden W and Potthoff M 2004 *Phys. Rev. B* **70** 235107
- [13] Davoudi B and Tremblay A-M S 2007 *Phys. Rev. B* **76** 085115
- [14] Vladimir M I and Moskalenko V A 1990 *Theor. Math. Phys.* **82** 301
- [15] Metzner W 1991 *Phys. Rev. B* **43** 8549
- [16] Pairault S, Sénéchal D and Tremblay A-M S 2000 *Eur. Phys. J. B* **16** 85
- [17] Sherman A 2018 *J. Phys.: Condens. Matter* **30** 195601
- [18] Sherman A 2020 *Eur. Phys. J. B* **93** 168
- [19] Sherman A 2020 *Phys. Scr.* **95** 095804
- [20] Kubo R 1962 *J. Phys. Soc. Jpn.* **17** 1100
- [21] Sherman A 2021 *J. Phys. Soc. Jpn.* **90** 104707
- [22] Abrikosov A A, Gor'kov L P and Dzyaloshinskii I E 1965 *Methods of Quantum Field Theory in Statistical Physics* (New York: Pergamon Press)

- [23] Schäfer T, Geles F, Rost D, Rohringer G, Arrigoni E, Held K, Blümer N, Aichhorn M and Toschi A 2015 *Phys. Rev. B* **91** 125109
- [24] Press W H, Teukolsky S A, Vetterling W T and Flannery B P 1995 *Numerical Recipes in Fortran* (Cambridge: Cambridge University Press) chapter 18
- [25] Jarrell M and Gubernatis J E 1996 *Phys. Rept.* **269** 133
- [26] Habershon S, Braams B J and Manolopoulos D E 2007 *J. Chem. Phys.* **127** 174108
- [27] Sherman A 2019 *Phys. Scr.* **94** 055802
- [28] Schmitt-Rink S, Varma C M and Ruckenstein A E 1988 *Phys. Rev. Lett.* **60** 2793
- [29] Ramšak A and Horsch P 1993 *Phys. Rev. B* **48** 10559
- [30] Sherman A and Schreiber M 1994 *Phys. Rev. B* **50** 12887
- [31] Slater J C 1951 *Phys. Rev.* **82** 538